# Leaves and sporangia developed in rare non-Fibonacci spirals in early leafy plants

# Title: Leaves and sporangia developed in rare non-Fibonacci spirals in early leafy plants

**Authors:** Holly-Anne Turner[1,†], Matthew Humpage[2], Hans Kerp[3], Alexander J. Hetherington[1]*

**Affiliations:**

[1]Institute of Molecular Plant Sciences, School of Biological Sciences, University of Edinburgh, Max Born Crescent, Edinburgh, EH9 3BF, UK.

[2]Northern Rogue Studios, 18 Hunsdon Road, Iffley, Oxford, OX4 4JE, UK.

[3]Research Group for Palaeobotany, Institute for Geology and Palaeontology, University of Münster, Heisenbergstrasse 2, 48149 Münster, Germany.

*Corresponding author. Email: sandy.hetherington@ed.ac.uk

†Present address: School of Biological, Earth and Environmental Sciences, University College Cork, Distillery Fields, North Mall, Cork, Ireland, T23 N73K

**Abstract:**

Lateral plant organs, including leaves and reproductive structures, are arranged on stems in distinct patterns, termed phyllotaxis. Most extant plants exhibit phyllotactic patterns that are mathematically described by the Fibonacci series. However, it remains unclear what lateral organ arrangements were present in early leafy plants. To investigate this, we quantified phyllotaxis in fossils of the Early Devonian lycopod *Asteroxylon mackiei*. We report diverse phyllotaxis in leaves, including whorls and spirals. Spirals were all n:(n+1) non-Fibonacci types. We also show that leaves and reproductive structures occurred in the same phyllotactic series, indicating developmental similarities between the organs. Our findings shed light on the longstanding debate about leaf origins and demonstrate the antiquity of non-Fibonacci spirals in plants.

**One-Sentence Summary:**

Diverse leaf arrangements identified in the earliest leafy plants, which differ from most extant species.

## Main Text:

Lateral plant organs such as leaves and reproductive structures are positioned on stems in a regular arrangement termed phyllotaxis. On theoretical grounds there could be a large number of possible phyllotactic patterns. However, this is not the case. A comparatively small number of discrete patterns are found in plants and spirals are the most common (*1–3*). When a leafy shoot with spiral phyllotaxis is viewed from above, adjacent leaves are arranged in clockwise and anticlockwise spirals that radiate out from the centre, and when viewed from the side these spirals form helices running around the circumference of the stem. Quantification of spiral phyllotaxis requires counting the numbers of clockwise and anticlockwise spirals, termed contact parastichies (*1*, *4*). Most commonly the number of clockwise and anticlockwise contact parastichies are integers in the Fibonacci sequence (1, 1, 2, 3, 5, 8, 13, 21…), and we will refer to these here as Fibonacci spirals. In a survey of angiosperms and gymnosperms, including 12,000 observations from 650 species, Fibonacci spirals occurred in >91% of observations (*1*, *3*). This number increased to >96% (*1*, *3*) when the duplicated Fibonacci series (2, 4, 6, 10, 16…) known as bijugate spirals (*1*, *5*) were included. Although there is some variation in the prevalence of Fibonacci spirals between different plant groups and between different organs (*3–6*) it remains the most common type of spiral phyllotaxis present in angiosperms, gymnosperms, ferns and two of the three groups of lycopods (*1*, *3–5*). Why Fibonacci spirals are so common in plants has perplexed scientists for centuries (*1*, *7–9*), but their evolutionary origin has been largely overlooked (*7*). Given the widespread occurrence of Fibonacci spirals in living species it was predicted that they were likely an ancestral and highly conserved characteristic of all seed plants (*7*) and likely all vascular plants (*4*, *10*, *11*). However, this hypothesis has not been vigorously tested (*5*, *6*, *12*), in part due to the difficulty of quantifying phyllotaxis in fossils. Thus, it remains unclear what phyllotactic types were present in early land plants and if Fibonacci spirals were as common in the geological past as they are today.

Here, we investigated phyllotaxis in fossils of *Asteroxylon mackiei* an Early Devonian lycopod, and member of the earliest clade of leafy plants, the Drepanophycales (*13–16*). Lycopod leaves, termed microphylls, evolved entirely independently from the leaves of euphyllophytes (*17–19*) suggesting that the evolution of leaf phyllotaxis was divergent in the two clades. Despite this independent evolution Fibonacci spirals are present in all three living clades of lycopods just as they are in the major groups of euphyllophytes (*5*). However, in members of the Lycopodiales, non-Fibonacci spirals are present at a much higher frequency than Fibonacci spirals (*4–6*, *20–24*). In some species such as *Lycopodium clavatum* and *Lycopodium annotinum*, Fibonacci spirals occur at a frequency of less than 1% (*5*, *20*). Whereas in others, Fibonacci spirals occur at a higher frequency but are only associated with a small number of developmental stages (*5*, *22*, *23*). Why non-Fibonacci spirals predominate in the Lycopodiales compared to the other two clades of living lycopods is a subject of ongoing debate (*6*, *20*, *23*) and it is currently unknown whether non-Fibonacci spirals in the Lycopodiales represent a derived or ancestral characteristic (*4*, *11*). Using a combination of classic fossil preparation techniques and 3D digital reconstruction methods we quantified phyllotaxis in multiple *A. mackiei* shoots to shed light on the origin of phyllotaxis in lycopod leaves.

### Quantification of *A. mackiei* phyllotaxis

To characterize phyllotaxis in *A. mackiei* we first took a centric approach (*1*), where leaf arrangement is characterized based on transverse sections close to the shoot apex. This approach

was made possible in *A. mackiei* due to the exceptional level of preservation of leafy shoots in the Rhynie chert (*14*, *16*, *25–27*). We identified *A. mackiei* apices in two previously published thin sections, Pb 4123 (*25*) and GLAHM Kid 2554 (*28*), and in two new preparations generated during this study (Fig. 1). To quantify phyllotaxis we represented the center point of each leaf by a point and connected neighboring leaves with both clockwise (red) and anti-clockwise (blue) spirals, termed contact parastichies (*4*). Phyllotaxis of each apex was then presented as a ratio of the number of clockwise and anti-clockwise contact parastichies, such as x:y where y>x. Based on our analysis we identified the phyllotactic patterns 5:5 (Fig. 1A), 6:6 (Fig. 1B), 7:8 (Fig. 1C) and 8:9 (Fig. 1D).Phyllotaxis differed between each specimen and included both spiral and whorled types. Whorled types contain equal numbers of clockwise and anti-clockwise contact parastichies (Fig. 1, A and B), whereas in spiral types they differ (Fig. 1, C and D) (*1*, *5*, *9*). The two specimens with spiral phyllotaxis 7:8 (Fig. 1C) and 8:9 (Fig. 1D) can both be described by the equation n:(n+1). n:(n+1) spiral phyllotaxis, where $n \geq 3$, is rare in living plants, and represents non-Fibonacci spirals (*1*, *3–5*). Based on our centric approach we demonstrated variable phyllotaxis in *A. mackiei* with both non-Fibonacci spirals and whorled types.

To investigate phyllotaxis further we took a cylindrical approach (*1*) by investigating leaf arrangement around the circumference of plant stems. We digitally reconstructed leafy shoots in 3D using serial peel preparations from the A. Bhutta Collection at the University of Cardiff (*29*). We digitally reconstructed three leafy shoots (Fig. 2). Fig. 2A, preserved an oblique section through a small leafy shoot, 4.1 mm in diameter, with only the front surface preserved. Fig. 2B, preserved a leafy shoot apex, the specimen was 5.8 mm in diameter, 28 mm long and included 62 well preserved leaves. Fig. 2C was the largest specimen, 46 mm long, 7.9 mm in diameter with 60 fully preserved leaves. Fig. 2C also preserved a lateral leafy shoot bud (Fig. 2C, arrowhead, Fig. S1). This lateral bud, along with small apices identified on the other two reconstructions (Fig. S1) demonstrates that lateral buds were common in *A. mackiei*. To quantify phyllotaxis in these specimens we used the software Blender to digitally ‘unwrap’ the stem to visualize 3D leaf arrangement as a 2D lattice (Fig. 2D-F). We represented the positions of leaves used for quantification by black points while grey points were used to denote leaves not included in the analysis. Fig. 2A only preserved the front surface of the axis so we could not quantify parastichies around the complete diameter of the specimen. However, based on the front portion we observed four successive horizontal whorls of leaves separated by internodes lacking leaves, which is consistent with a whorled arrangement (Fig. 2G). For the other two specimens, for which leaves extended around the full circumference of the shoots, we annotated the lattice diagrams with both clockwise (red) and anticlockwise (blue) contact parastichies. Based on this analysis we recognized phyllotaxis as 7:8 (Fig. 2B) and 4:5 (Fig. 2C), both non-Fibonacci n:(n+1) spirals. As with our centric analysis, we again recognized both spiral and whorled phyllotaxis in *A. mackiei*.

To further build on our investigation we next quantified phyllotaxis using both a centric and cylindrical approach within a single specimen. To achieve this we leveraged our 3D reconstruction of a shoot apex Fig. 2B. Although the original peel preparations used to reconstruct Fig. 2B were longitudinal sections (Fig. 3A), we predicted that it would be possible to create a virtual transverse section necessary for a centric investigation of phyllotaxis. Using the software Blender we first filled holes within our original skeletal model (Fig. 3B) and smoothed pixilated regions of the apex. This step allowed us to clearly visualize the dense clustering of leaves at the apex (Fig. 3C). Next we cut a digital transverse section through the apex, allowing us to quantify phyllotaxis (Fig. 3D). At the center of the apex a 7:7 phyllotaxis was apparent. However, when the parastichies are followed outwards from the center, one of the

anticlockwise parastichies splits resulting in the 7:8 phyllotaxis observed when using a cylindrical approach (Fig. 3E, F Fig.2E, Fig. S2). This shoot apex therefore preserves evidence of a transition between whorled and spiral phyllotaxis. Taken together our analysis of phyllotaxis in *A. mackiei* indicated that phyllotaxis was highly diverse consisting of spirals and whorls, that spirals were non-Fibonacci n:(n+1) types, and that transitions in phyllotaxis were possible in a single leafy shoot.

## Comparison of *A. mackiei* phyllotaxis with extant species

Based on studies of extant species alone, it was predicted that Fibonacci spirals were likely an ancestral and highly conserved characteristic of all major groups of vascular plants (*4*, *10*, *11*). Our findings from *A. mackiei* do not support this hypothesis. Instead they indicate that n:(n+1) non-Fibonacci types were present early in land plant evolution despite being a rare phyllotactic type in living species (*1*, *3–5*).There are at least two groups of living plants where non-Fibonacci n:(n+1) spirals occur more commonly; some species of cacti (*4*, *30*, *31*) and members of the Lycopodiales (*4–6*, *20–24*). Given that both *A. mackiei* and the Lycopodiales are members of the lycopods (*13*), we sought to interpret our new findings specifically in the context of lycopod evolution. Extant lycopods consist of three clades; the Lycopodiales, Selaginellales and Isoetales (*32*). In members of the Isoetales all reported spiral phyllotaxis is Fibonacci (*6*, *33*, *34*). In the Selaginellales, spiral phyllotaxis occurs in the Homoeophyllae and *Selaginella selaginoides* clades (*35*). Spirals are Fibonacci in the larger Homoeophyllae clade with only the single species *S. selaginoides* reported as developing more complex spirals (*6*). However, detailed characterization of 10 members of the Lycopodiales demonstrate that they share all the characteristics of *A. mackiei* phyllotaxis described here, including, high variability, regular transitions in phyllotaxis and the almost exclusive development of non-Fibonacci spirals including n:(n+1) types (*4–6*, *20–24*). Based on investigations of living species and fossils from the Carboniferous, Church (*4*, *11*) predicted that the non-Fibonacci n:(n+1) spirals found in living Lycopodiales were a derived condition from an ancestor with Fibonacci spirals. However, our findings from *A. mackiei*, a member of the extinct Drepanophycales, challenge this hypothesis and instead suggest that non-Fibonacci n:(n+1) spirals and whorls were ancestral in lycopods. Evidence for this hypothesis includes data presented here for *A. mackiei*, the low frequency of Fibonacci spirals in living Lycopodiales, and the absence of Fibonacci spirals from other fossil lycopods such as Early Carboniferous *Oxroadia* species (*36*, *37*). To our knowledge the earliest reports of Fibonacci spirals in lycopods are in arborescent taxa in the Carboniferous (*11*, *38*), suggesting a late origin of Fibonacci spirals in lycopods. Lycopods were the earliest group of leafy plants therefore suggesting that non-Fibonacci spirals in leaves predated the widespread occurrence of Fibonacci spirals in land plants. Finally, because leaves evolved independently in lycophytes and euphyllophytes (*17–19*) and non-Fibonacci types appear ancestral in lycophytes this suggests that Fibonacci spirals present in living members of both groups may have evolved independently. Collectively our analysis of *A. mackiei* leaves changes our interpretation of the evolution of phyllotaxis in lycopods and demonstrates the antiquity of non-Fibonacci spirals.

The identification of the antiquity of non-Fibonacci spirals in lycopods begs the question of why non-Fibonacci spirals are present in members of the Lycopodiales and *A. mackiei* but are found less frequently in other groups of vascular plants (*1*, *3–5*). Based on studies of extant

members of the Lycopodiales, a number of hypotheses have been put forward to explain the higher occurrence of non-Fibonacci spirals. These include predictions related to the shape or organization of the meristem, relative size of leaf primordia compared to the apex, the presence of dichotomous branching, or different regulation of phyllotaxis in lycopods compared to euphyllophytes (*5*, *6*, *20*, *23*). Of these, dichotomous branching is considered the most likely cause (*6*, *20*, *23*) due to the major changes to meristem size and shape involved in branching and associated restriction of the sites for new primordia development (*6*, *23*, *39*, *40*). In support of this hypothesis is the observation that non-Fibonacci spirals occur at higher frequencies in euphyllophytes with dichotomous branching (*31*, *39*, *40*), and dichotomous branching was common in *A. mackiei,* (*15*, *16*). The link between dichotomous branching and non-Fibonacci spirals does not hold true for all species including members of the Selaginellales, or in palms (*5*, *6*, *40*, *41*) suggesting it is not the only contributing factor to the development of non-Fibonacci spirals. However, if dichotomous branching is correlated with the development of non-Fibonacci spirals in land plants it suggests that non-Fibonacci spirals may have been more frequent during the early diversification of vascular plants from the Silurian to the Carboniferous when dichotomous branching was more common than today (*42*). The analysis of phyllotaxis in the fossil record therefore represent a key line of evidence for uncovering the evolutionary history of Fibonacci spirals in land plants.

**Phyllotaxis of leaves and sporangia in a fertile *A. mackiei* shoot**

Having characterized phyllotaxis in *A. mackiei* leaves and drawn conclusions concerning the evolution of phyllotaxis, we finally wanted to use our analysis to investigate a related question, the origin of leaves. The origin of leaves in lycophytes has been debated for over a century with two major competing hypotheses in the literature. The enation hypothesis predicts that leaves evolved as *de novo* structures on the shoot and the sterilization hypothesis predicts that leaves evolved by the sterilization of sporangia (*13*, *17*, *43–47*). *A. mackiei* leaves were traditionally interpreted as supporting the enation hypothesis for leaf origins (*44*). This is because the leaves of *A. mackiei* only developed a vascular trace that extended to the leaf base rather than along the full length of the leaf as in other lycopods (*13*, *16*, *25*, *27*, *29*). The leaves of *A. mackiei* were therefore interpreted as a transitional stage between un-vascularized enations and fully vascularized leaves (*44*). However, subsequent detailed cladistic analysis of early lycophytes, including *A. mackiei*, instead suggests that the leaves of *A. mackiei* are homologous to leaves of all lycopods and the absence of the leaf trace in *A. mackiei* is due to a secondary loss (*13*, *17*, *45*). We investigated the phyllotactic relationships between leaves and sporangia to help evaluate the enation and sterilization hypotheses. To investigate phyllotaxis in both sporangia and leaves we reconstructed a fertile shoot of *A. mackiei* (Fig. 4). Unlike in living lycopods, where sporangia are always positioned on the adaxial sides of specialized leaf like structures termed sporophylls (*48*), sporangia of *A. mackiei* were borne laterally on stems connected by short stalks (*25*). Sporangia of *A. mackiei* could be readily differentiated from leaves due to their larger size, prominent vascular trace and valvate tips or abscission marks (*25*) (Fig. 4A, orange arrowheads).

The fertile region consisted of 19 sporangia and 118 small and densely packed leaves. We quantified phyllotaxis taking a cylindrical approach using a conical lattice due to the different diameters at the top and base of the axis (Fig. 4C and D). On the lattice we first plotted the position of the sporangia. Based solely on sporangia we were unable to identify any regular phyllotactic arrangement. We next investigated leaves and sporangia together. Based primarily on the positions of leaves we identified a 15:16 spiral phyllotaxis, and importantly, the position of the sporangia were included in this phyllotactic pattern. This suggests that leaves and

sporangia developed in a single phyllotactic series, and can be considered as topographically homologous (*49*). Taken together, the lack of phyllotaxis in sporangia when examined in isolation, but their incorporation with leaves into a recognizable n:(n+1) spiral highlights the developmental similarity between the two organs.

The occurrence of leaves and sporangia in the same phyllotactic series alone does not allow us to conclusively reject either the enation or sterilization hypothesis. Shared development could result from either shared origin of the two organs (sterilization hypothesis) or convergence on the same developmental patterning mechanism for two distinct organs (enation hypothesis). However, our findings do add to a growing body of evidence in support of the sterilization hypothesis. Previous support for the sterilization hypothesis suggests that this is a developmentally parsimonious interpretation for leaf evolution because it does not require the evolution of a new organ system, and leaves and sporangia share developmental similarities, including similarities in gene expression (*13*, *17*, *45*, *46*). Development in the same phyllotactic series of both sporangia and leaves in *A. mackiei* adds a further point of similarity between the two organs, consistent with the sterilization hypothesis (*13*, *17*, *45*, *46*). Our quantitative assessment of phyllotaxis in a fertile apex therefore adds evidence to the longstanding debate about the origin of leaves in lycophytes.

## References and Notes

1. R. V. Jean, *Phyllotaxis* (Cambridge University Press), 1994.
2. R. D. Meicenheimer, "Decussate to spiral transitions in phyllotaxis" in *Symmetry in Plants*, R. V. Jean, D. Barabé, Eds. (1998), 125–143.
3. R. V. Jean, Model testing in phyllotaxis. *J. Theor. Biol.* **156**, 41–62 (1992).
4. A. H. Church, *On the relation of phyllotaxis to mechanical laws* (Williams & Norgate, London, 1904).
5. E. M. Gola, A. Banasiak, Diversity of phyllotaxis in land plants in reference to the shoot apical meristem structure. *Acta Soc. Bot. Pol.* **85**, 1–21 (2016).
6. J. C. Schoute, *Manual of Pteridology* (Martinus Nijhoff, The Hague, The Netherlands, 1938).
7. D. Reinhardt, E. M. Gola, Law and order in plants – the origin and functional relevance of phyllotaxis. *Trends Plant Sci.* **27**, P1017-1032 (2022).
8. I. Adler, D. Barabé, V. Jean, R, A history of the study of phyllotaxis. *Ann. Bot.* **80**, 231–244 (1997).
9. X. Yin, Phyllotaxis: from classical knowledge to molecular genetics. *J. Plant Res.* **134**, 373–401 (2021).
10. R. V. Jean, Phyllotactic pattern generation: a conceptual model. *Ann. Bot.* **61**, 293–303 (1988).
11. A. H. Church, *On the interpretation of phenomena of phyllotaxis* (Oxford University Press, London (UK), 1920).
12. E. Véron, T. Vernoux, Y. Coudert, Phyllotaxis from a single apical cell. *Trends Plant Sci.* **26**, 124–131 (2021).

13. P. Kenrick, P. R. Crane, *The origin and early diversification of land plants: a cladistic study* (Smithsonian Series in Comparative Evolutionary Biology. Washington, DC, USA: Smithsonian Institute Press, 1997).

14. D. Edwards, Embryophytic sporophytes in the Rhynie and Windyfield cherts. *Trans. R. Soc. Edinburgh, Earth Sci.* **94**, 397–410 (2004).

15. A. J. Hetherington, S. L. Bridson, A. Lee Jones, H. Hass, H. Kerp, L. Dolan, An evidence-based 3D reconstruction of *Asteroxylon mackiei*, the most complex plant preserved from the Rhynie chert. *Elife*. **10**, e69447 (2021).

16. R. Kidston, W. H. Lang, On Old Red Sandstone plants showing structure, from the Rhynie Chert Bed, Aberdeenshire. Part III. *Asteroxylon mackiei*, Kidston and Lang. *Trans. R. Soc. Edinb. Earth Sci.* **52**, 643–680 (1920).

17. P. R. Crane, P. Kenrick, Diverted development of reproductive organs: A source of morphological innovation in land plants. *Plant Syst. Evol.* **206**, 161–174 (1997).

18. C. K. Boyce, The evolution of plant development in a paleontological context. *Curr. Opin. Plant Biol.* **13**, 102–107 (2010).

19. A. M. F. Tomescu, Megaphylls, microphylls and the evolution of leaf development. *Trends Plant Sci.* **14**, 5–12 (2009).

20. E. Gola, Phyllotaxis diversity in *Lycopodium clavatum* L. and *Lycopodium annotinum* L. *Acta Soc. Bot. Pol.* **65**, 235–247 (1996).

21. D. W. Stevenson, Observations on phyllotaxis, stelar morphology, the shoot apex and gemmae of *Lycopodium lucidulum* Michaux (Lycopodiaceae). *Bot. J. Linn. Soc.* **72**, 81–100 (1976).

22. E. Vindt-Balguerie, Phyllotaxie et ramification du jeune *Huperzia selago* issu du développement de la bulbille. *Bull. la Société Bot. Fr. Actual. Bot.* **138**, 135–146 (1991).

23. X. Yin, R. D. Meicenheimer, The ontogeny, phyllotactic diversity, and discontinuous transitions of *Diphasiastrum digitatum* (Lycopodiaceae). *Am. J. Bot.* **104**, 8–23 (2017).

24. R. Rutishauser, "Plastochrone ratio and leaf arc as parameters of a quantitative phyllotaxis analysis in vascular plants" in *Symmetry in Plants*, R. V. Jean, D. Barabé, Eds. (World Scientific Publishing Co. Pte. Ltd, Singapore, 1998. 171–212.

25. H. Kerp, C. H. Wellman, M. Krings, P. Kearney, H. Hass, Reproductive organs and in situ spores of *Asteroxylon mackiei* Kidston & Lang, the most complex plant from the Lower Devonian Rhynie Chert. *Int. J. Plant Sci.* **174**, 293–308 (2013).

26. H. Kerp, Organs and tissues of Rhynie chert plants. *Philos. Trans. R. Soc. B Biol. Sci.* **373**, 20160495 (2018).

27. F. M. Hueber, Thoughts on the early lycopsids and zosterophylls. *Ann. Missouri Bot. Gard.* **79**, 474–499 (1992).

28. R. Kidston, W. H. Lang, On Old Red Sandstone plants showing structure, from the Rhynie Chert Bed, Aberdeenshire. Part IV. Restorations of the vascular cryptogams, and discussion of their bearing on the general morphology of the Pteridophyta and the origin of the organisation of land-plants. *Trans. R. Soc. Edinb. Earth Sci.* **52**, 831–854 (1921).

29. A. A. Bhutta, Studies on the Flora of the Rhynie Chert. University of Wales. (1969).

30. J. D. Mauseth, Shoot apical meristem stability and non-Fibonacci phyllotaxy in ribbed cacti. *Int. J. Plant Sci.* **181**, 518–528 (2020).

31. E. Gola, Phyllotactic spectra in cacti: *Mammilaria* species and some genera from *Rebutia* group. *Acta Soc. Bot. Pol.* **66**, 237–257 (1997).

32. PPG I, A community-derived classification for extant lycophytes and ferns. *J. Syst. Evol.* **54**, 563–603 (2016).

33. W. F. B. Hofmeister, *On the Germination, Development, and Fructification of the Higher Cryptogamia: And on the Fructification of the Coniferæ. Translated to English by Frederick Currey* (London (UK), 1862.

34. C. West, H. Takeda, X. On *Isoetes japonica*, A. Br. *Trans. Linn. Soc. London. 2nd Ser. Bot.* **8**, 333–376 (1915).

35. X.-M. Zhou, C. J. Rothfels, L. Zhang, Z.-R. He, T. Le Péchon, H. He, N. T. Lu, R. Knapp, D. Lorence, X.-J. He, X.-F. Gao, L.-B. Zhang, A large-scale phylogeny of the lycophyte genus *Selaginella* (Selaginellaceae: Lycopodiopsida) based on plastid and nuclear loci. *Cladistics*. **32**, 360–389 (2016).

36. R. M. Bateman, Morphometric reconstruction, palaeobiology and phylogeny of *Oxroadia gracilis* Alvin emend. and *O. conferta* sp. nov.: anatomically-preserved rhizomorphic lycopsids from the Dinantian of Oxroad Bay, SE Scotland. *Palaeontogr. Abteilung B*. **228**, 29–103 (1992).

37. K. L. Alvin, A new fertile lycopod from the Lower Carboniferous of Scotland. *Palaeontology*. **8**, 281–293 (1965).

38. A. Dickson, II. On the phyllotaxis of *Lepidodendron*. *Trans. Bot. Soc. Edinburgh*. **11**, 145–147 (1873).

39. B. Zagórska-Marek, Phyllotactic patterns and transitions in *Abies balsamea*. *Can. J. Bot.* **63**, 1844–1854 (1985).

40. E. M. Gola, Dichotomous branching: the plant form and integrity upon the apical meristem bifurcation. *Front. Plant Sci.* **5**, 1–7 (2014).

41. P. B. Tomlinson, The shoot apex and its dichotomous branching in the *Nypa* palm. *Ann. Bot.* **35**, 865–879 (1971).

42. G. Chomicki, M. Coiro, S. S. Renner, Evolution and ecology of plant architecture: integrating insights from the fossil record, extant morphology, developmental genetics and phylogenies. *Ann. Bot.* **120**, 855–891 (2017).

43. F. O. Bower, *The origin of a land flora* (Macmillan and Co., Limited, London (UK), 1908).

44. F. O. Bower, *Primitive land plants-also known as the Archegoniatae* (Macmillan and Co., Limited, London, 1935).

45. P. Kenrick, "The telome theory" in *Developmental genetics and plant evolution*, Q. C. B. Cronk, R. M. Bateman, J. Hawkins, Eds. (Taylor & Francis, London, 2002), pp. 365–387.

46. A. Vasco, T. L. Smalls, S. W. Graham, E. D. Cooper, G. K. K.-S. Wong, D. W. Stevenson, R. C. Moran, B. A. Ambrose, Challenging the paradigms of leaf evolution: Class III HD-Zips in ferns and lycophytes. *New Phytol.* **212**, 745–758 (2016).

47. C. J. Harrison, M. Rezvani, J. A. Langdale, Growth from two transient apical initials in the meristem of Selaginella kraussiana. *Development*. **134**, 881–889 (2007).

48. D. W. Bierhorst, *Morphology of vascular plants* (Macmillan, New York (USA), 1971).

49. E. G. Cutter, "Patterns of organogensis in the shoot" in *Trends in plant morphogenesis: essays presented to C. W. Wardlaw on his sixty-fifth birthday*, E. G. Cutter, Ed. (Longmanns, Green and Co. LTD., London (UK), 1966), pp. 220–234.

50. A. J. Hetherington, H.-A. Turner, *Asteroxylon mackiei* 3D reconstructions for investigation of phyllotaxis. *Univ. Edinburgh. Sch. Biol. Sci. Inst. Mol. Plant Sci.* (2023), doi:https://doi.org/10.7488/ds/3808.

51. M. Sutton, R. Garwood, D. Siveter, D. Siveter, SPIERS and VAXML: A software toolkit for tomographic visualisation and a format for virtual specimen interchange. *Palaeontol. Electron.* ***15***, 1–14.

52. L. E. Meade, A. R. G. Plackett, J. Hilton, Reconstructing development of the earliest seed integuments raises a new hypothesis for the evolution of ancestral seed-bearing structures. *New Phytol.* **229**, 1782–1794 (2021).

**Acknowledgments:**

We would like to thank Dianne Edwards and Chris Berry for access to the A. Bhutta collection at the University of Cardiff. This invaluable assistance allowed the project to be carried out during the pandemic. We thank Neil Clark for access to the Kidston Collection. We thank Nick Fraser, Andy Ross and Yves Candela for assistance accessioning material into National Museums Scotland. We thank Francis Buckley and North Sea Core for their assistance with Rhynie chert specimens. We thank five reviewers for constructive comments on the manuscript.

**Funding:**

UK Research and Innovation Future Leaders Fellowship MR/T018585/1 (AJH)

Royal Society research grant RGS\R2\212063 (AJH)

Deutsche Forschungsgemeinschaft KE 584/13- 1 (HK)

Deutsche Forschungsgemeinschaft KE 584/13- 2 (HK)

**Author contributions:**

Conceptualization: AJH

Methodology: AJH, H-AT, MH

Investigation: H-AT, AJH, MH, HK

Visualization: H-AT, AJH, MH, HK

Funding acquisition: AJH, HK

Supervision: AJH

Writing – original draft: AJH, H-AT

Writing – review & editing: H-AT, AJH, MH, HK

**Competing interests:** Authors declare that they have no competing interests.

**Data and materials availability:**

Fossil specimens described in this study are deposited in four collections. Collection abbreviations: Forschungsstelle für Paläobotanik, Institut für Geologie und Paläontologie, University of Münster, Münster, Germany; Pb. The Hunterian, University of Glasgow; GLAHM. National Museums Scotland; NMS. Akhlaq Ahmed Bhutta peel collection, University of Cardiff; A. Bhutta. Accession numbers for all figured specimens are: Pb 4123 (Fig. 1A), Pb 5022 (Fig. 1B), GLAHM Kid 2554 (Fig. 1C), NMS G.2022.15.1 (Fig. 1D), A. Bhutta BL29A/40 (Fig. 3A), A. Bhutta XYA/29 (Fig. 4A). 3D reconstructions are based on peel numbers A. Bhutta 139A/2-072 (Fig. 2A), A. Bhutta BL29A/15-090 (Fig. 2B, Fig. 3), A. Bhutta BL29A/ 50-182 (Fig. 2C) and A. Bhutta XYA/4-181 (Fig. 4B). Cropped and aligned images of peels used to generate 3D reconstructions, are deposited on Edinburgh University DataShare (*50*), as are the 3D reconstructions. An interactive 3D model of the specimen Fig. 3B can be viewed on Sketchfab: https://sketchfab.com/3d-models/asteroxylon-mackiei-f090e445a53a47cd8b394b1ee7d9f517 (Password Asteroxylon). All other data are available in the main text or the supplementary materials.

**Supplementary Materials**

Materials and Methods

Figs. S1 to S3

References (*51*, 52)

Data S1

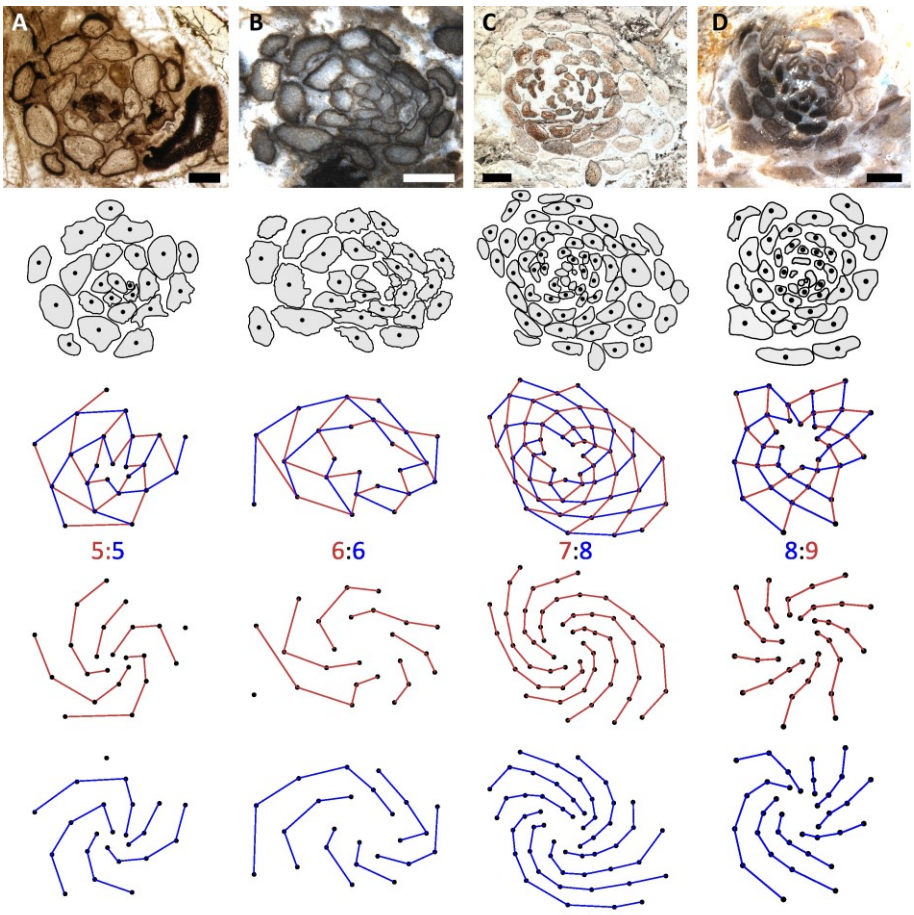


**Fig. 1. Phyllotactic diversity in *A. mackiei* based on a centric investigation of shoot apices.** (**A-D**) Row 1, transverse sections of four *A. mackiei* apices. Row 2, line drawing made from A-D, showing leaves in grey and the center of all leaves included in the analysis marked with a black point. Row 3-5, clockwise (red) and anti-clockwise (blue) contact parastichies. Specimen accession codes: Pb 4123 (A), Pb 5022 (B), GLAHM Kid 2554 (C), NMS G.2022.15.1 (D). Scale bars, 1 mm.

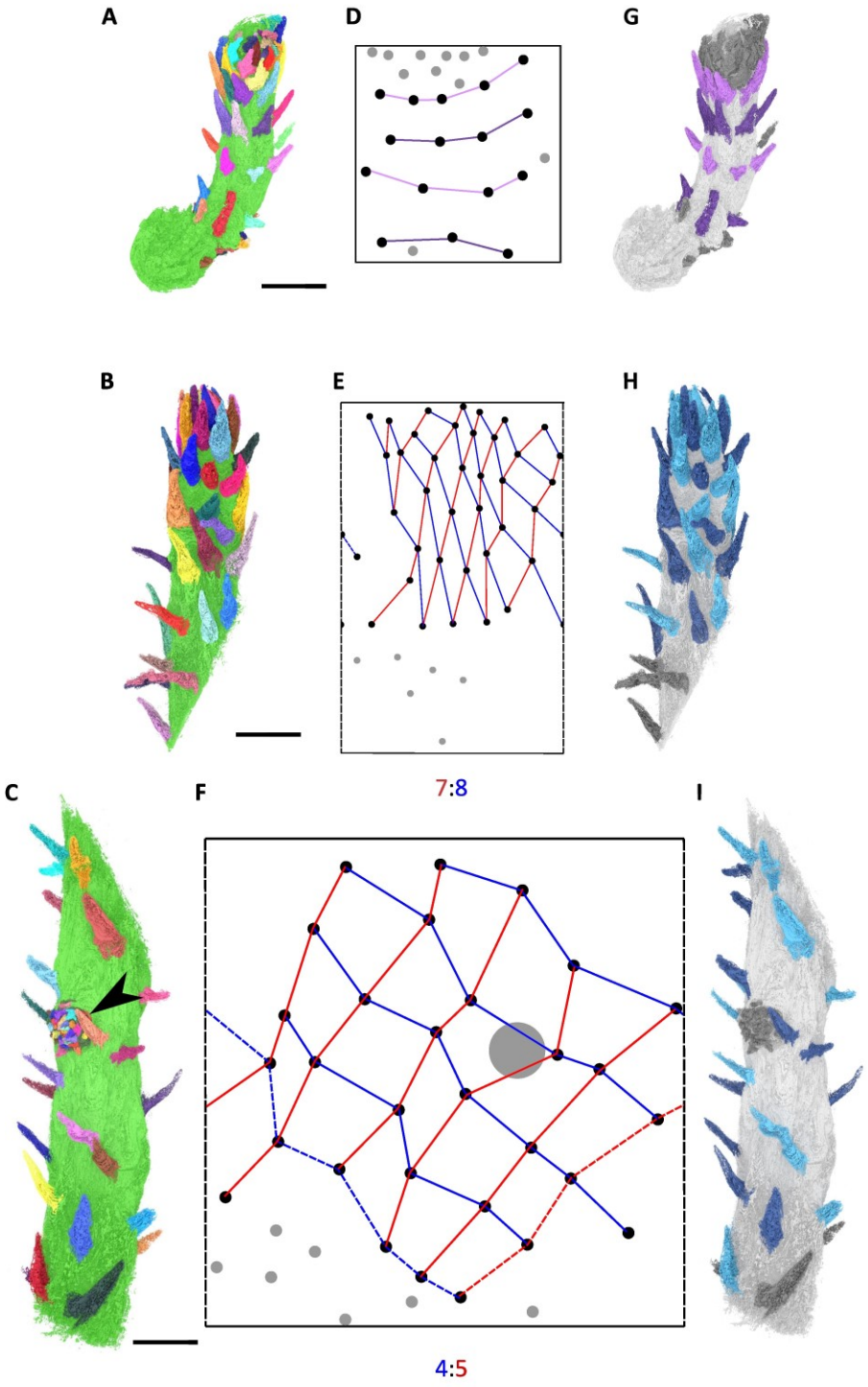


**Fig. 2. Cylindrical quantification of phyllotaxis based on 3D digital reconstructions of leafy shoots.** (**A-C**) 3D digital reconstruction of *A. mackiei* leafy shoots showing leaves randomly colored, black arrow in C marks lateral bud. (**D-F**) 3D leaf arrangement represented on a 2D lattice with points representing leaf positions and lines representing contact parastichies, red (clockwise), blue (anticlockwise). Dashed lines represent continuations of parastichies from one side of the lattice to the other. Black points are leaves included in lattice and grey points indicate

leaves, or putative leaves excluded from the analysis. Large grey circle in F marks position of the bud. (**G-I**) 3D digital models with leaves colored to highlight phyllotaxis. (G) Alternating light and dark purple leaves indicate successive whorls. (H, I) Alternating light and dark blue leaves indicate successive anticlockwise contact parastichies. Scale bars, 5 mm.

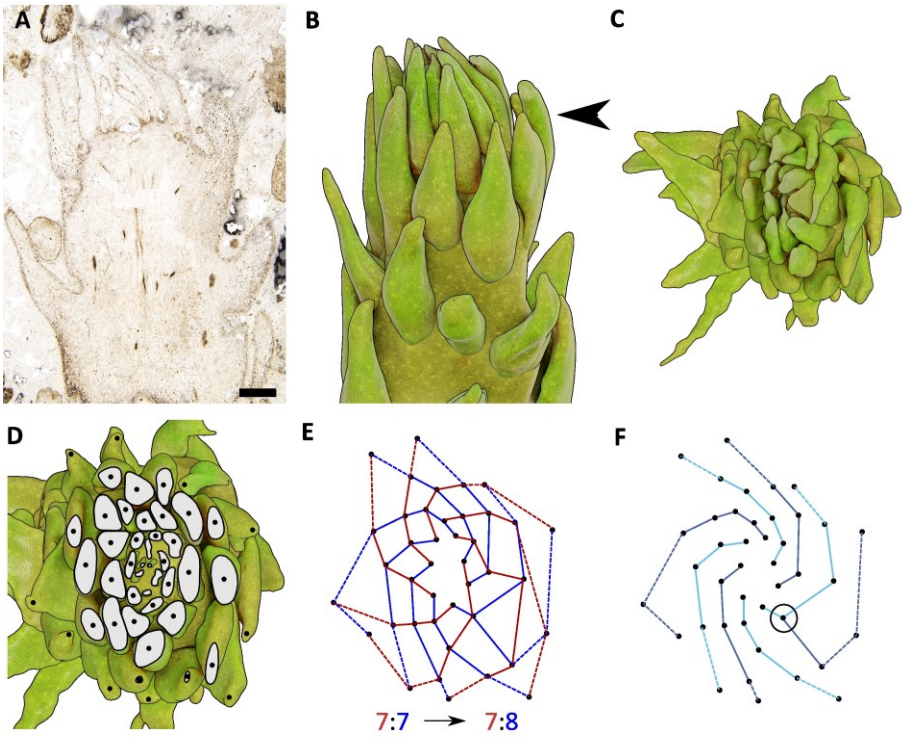


**Fig. 3. Evidence of a phyllotactic transition within *A. mackiei*.** (**A**) Peel used to create 3D model showing a longitudinal section through the shoot apex. (**B**, **C**), 3D digital rendering of a side-on (B) and top-down (C) view of the apex shown in Fig. 2B. (**D**) Virtual transverse section made through the apex at position marked by the black arrow in B. Leaves cut in transverse section are shown in grey with black points indicating the center of sectioned leaves and un-sectioned leaf tips very close to the apex. (**E**) Lattice diagram of leaf arrangement based on D showing clockwise (red) and anti-clockwise (blue) contact parastichies. Solid lines connect leaves cut in transverse section in D, and dotted lines connect leaves just below the plane of section. (**F**) Dark and light blue lines show successive anti-clockwise parastichies, with the circled leaf marking the transition from 7 to 8 anti-clockwise contact parastichies. Specimen accession code: A. Bhutta BL29A/40 (A). Scale bar, 1 mm.

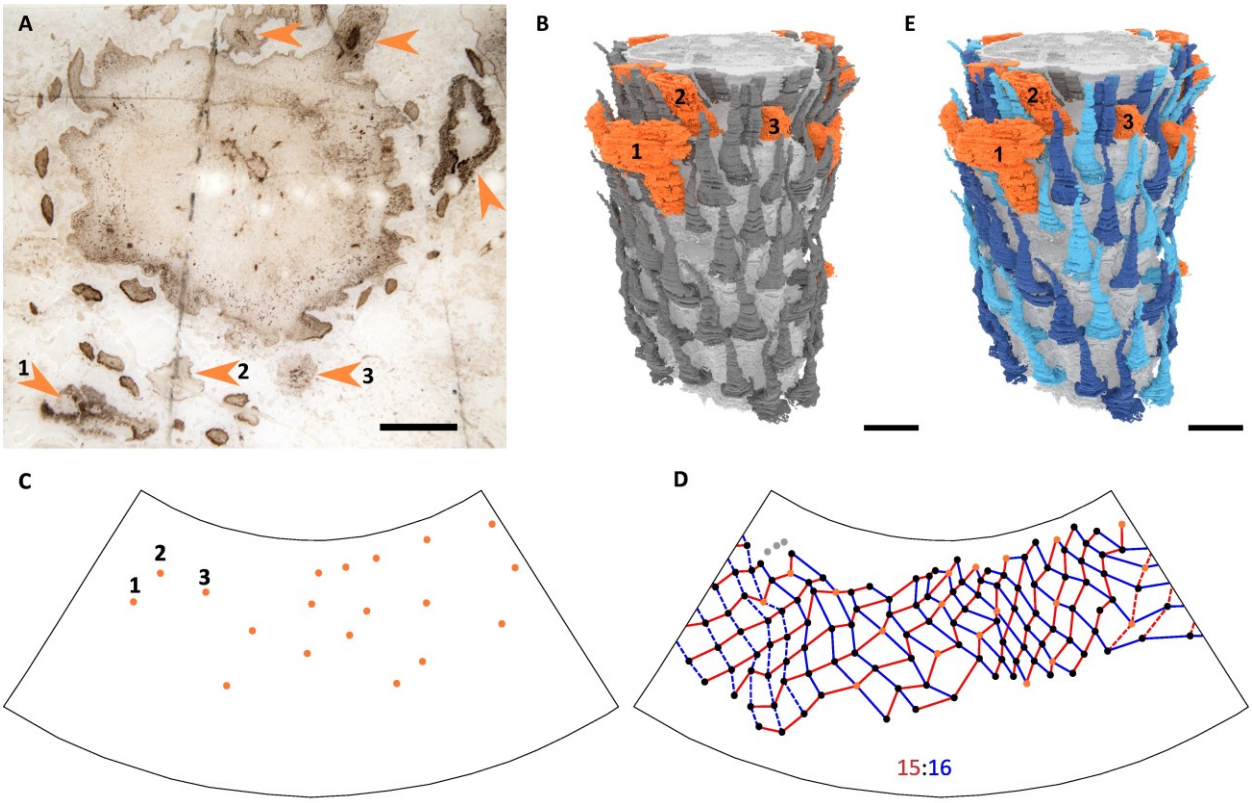


**Fig. 4. *A. mackiei* sporangia are arranged in the same phyllotactic series as leaves**. (**A**) Peel used to create the 3D model showing a transverse section of the stem with six sporangia surrounding the axis (orange arrowheads). Numbered arrowheads 1-3, highlight the position of three sporangia in A-C and E. (**B**) 3D digital reconstruction of the fertile leafy shoot, with leaves in dark grey and sporangia in orange. (**C**) 3D arrangement of sporangia represented on a 2D lattice. (**D**) 2D lattice depiction of all leaves and sporangia. Orange points are sporangia, black points are leaves included in lattice and grey points indicate leaves, or putative leaves, excluded from the analysis. Contact parastichies are marked with red (clockwise), blue (anticlockwise) lines. (**E**) 3D digital model with leaves colored in alternating light and dark blue to highlight successive anticlockwise parastichies. Specimen accession code: A. Bhutta XYA/29 (A). Scale bars, 2 mm.

# Supplementary Materials for

## Leaves and sporangia developed in rare non-Fibonacci spirals in early leafy plants

Holly-Anne Turner, Matthew Humpage, Hans Kerp, Alexander J. Hetherington

Correspondence to: sandy.hetherington@ed.ac.uk

**This PDF file includes:**

Materials and Methods
Figs. S1 to S3

**Other Supplementary Materials for this manuscript include the following:**

Data S1

## Materials and Methods

Specimen accession code abbreviations: Forschungsstelle für Paläobotanik, Institut für Geologie und Paläontologie, University of Münster, Münster, Germany; Pb. The Hunterian, University of Glasgow; GLAHM. National Museums Scotland; NMS. Akhlaq Ahmed Bhutta peel collection, University of Cardiff; A. Bhutta.

Rhynie chert specimens

Rhynie chert specimens preserving *Asteroxylon mackiei* used in this study came from five sources. Two specimens were reinvestigations of previously published thin sections, Pb 4123 (*25*) (Fig. 1A), and GLAHM Kid 2554 (*28*) (Fig. 1C). One specimen Pb 5022 (Fig. 1B), was identified on an isolated block of Rhynie chert in the collections of the Forschungsstelle für Paläobotanik, Institut für Geologie und Paläontologie, University of Münster, Münster, Germany. This specimen was a small fragment of a block collected from a trench dug in 1964, used in previous descriptions of *A. mackiei* (*15*, *25*). A separate specimen NMS G.2022.15.1 (Fig. 1D), was identified in collections of Rhynie chert in the lab of AJH at the University of Edinburgh and is now accessioned into National Museum Scotland. The material was originally collected in farmland owned by the Windyfield Farm (NJ 349642 mE, 827852 mN) adjacent to the site of special scientific interest (SSSI) by a local land owner before 2021. Specimens were passed to North Sea Core to help distribute the samples for academic research with the mutual agreement of NatureScot. Blocks were distributed using the accession numbers North Sea Core NSC.01-NSC.45. Specimen NMS G.2022.15.1, was identified on a small fragment of NSC.10, and the remainder of NSC.10 is currently being processed in the lab of AJH. Finally, all peels used in the study for 3D reconstructions were from the A. Bhutta peel collection at the University of Cardiff (*29*). In all cases *A. mackiei* was readily identified due to its characteristic stellate xylem, leaf traces and as it is the only leafy plant preserved in the Rhynie chert.

Imaging of Rhynie material

GLAHM Kid 2554 originally described by Kidston and Lang (*28*) was imaged using a Zeiss Axioscope 7 at The Hunterian, University of Glasgow. Specimen PB 4123 was reinvestigated based on images taken by HK as part of Kerp et al., (*25*). Specimens Pb 5022, (Fig. 1B), NMS G.2022.15.1 (Fig. 1D), and the figured peel specimens (Fig. 3A, 4A, S1 B, C, E, F, I) were imaged under cross polarized reflected light from a Schott VisiLED ring light using a Nikon SMZ18. All peels used for the 3D reconstructions were scanned at 94.4882 pixels/mm using an Epson perfection v600 scanner.

3D reconstructions using SPIERS

*A. mackiei* leafy shoots were digitally reconstructed from serial acetate peels from the A. Bhutta collection (*29*). The list of peels used in each reconstruction are listed in Data S1. The peels in the A. Bhutta collection were made using 0.075 mm acetate sheets, with peels either mounted on card using sellotape or mounted on glass slides with cover slips (*29*). All peels were first scanned using an Epson perfection v600 scanner, then digital reconstructions were carried out in SPIERS (*51*). Images of peels were first manually aligned using SPIERSalign (*51*) before being cropped to the leafy shoots of interest (cropped aligned images are deposited on Edinburgh University DataShare (*50*)). The aligned series of images were then imported into SPIERSedit (*51*). Due to the historic nature of the peels and the variability in preservation between specimens manual thresholding (using greyscale values between 100-180) were applied to each peel. Additionally,

the brush tool was used to increase the brightness of plant tissue not visible after thresholding. Once thresholding of images was complete, shoots, leaves and sporangia were all masked separately before 3D reconstructions were generated in SPIERSview (*51*).

To create the 3D models it was essential to estimate the thickness of each peel. Despite generating over 2000 peels from multiple blocks in his work Bhutta (*29*) only provided a single estimate of average peel thickness, 0.058 mm. For reconstruction Fig. 4B where no other estimate of thickness could be made, a peel thickness of 0.058 mm was used. However, for Fig.2A-C, where peels were longitudinal sections of leafy shoots, we took an additional approach to estimate peel thickness. We predicted that *A. mackiei* leafy shoots were cylindrical (consistent with evidence from well preserved transverse sections of axes (*16*, *28*)), and therefore if we could measure stem diameter directly from longitudinal sections we could calculate a more realistic estimate of peel thickness for each specimen. We measured stem diameter based on well preserved longitudinal peel sections allowing us to calculate an average stem diameter for each specimen. Next, we counted the number of peels that traversed the full width of the stem. By dividing our measured stem diameter by the number of peels used to traverse the width of the stem we could estimate peel thickness for each leaf shoot (Data S1). Based on this we estimated peel thicknesses of 0.0594 mm (Fig. 2A), 0.143 mm (Fig. 2B) and 0.099 mm (Fig. 2C) (Data S1). This analysis revealed that Fig. 2A, was very close to the average thickness estimated by Bhutta (*29*). However, for both Fig. 2B, C, our analyses indicated that peel thickness was likely much thicker than Bhutta's estimate (*29*). Using the 0.058 mm average peel thickness provided by Bhutta (*29*) generated stem reconstructions that were significantly compressed (Fig. S3). From examining the *A. mackiei* plant tissues, the surrounding plants and peaty substrate we could see no evidence for extensive compression. We therefore predicted that the most likely explanation was that both leafy shoots were closer to being cylindrical, and therefore that peel thickness was more than Bhutta's original value. Our approach therefore allowed us to generate reconstructions that were more cylindrical, which we believe were more accurate than the flattened reconstructions. A similar method was used by Meade et al., (*52*) who also experienced issues when reconstructing 3D digital models from historic peels. Finally, we exported our 3D models to Blender for imaging and all 3D reconstructions are deposited on Edinburgh University DataShare (*50*).

Digital transverse section

To quantify phyllotaxis in Fig. 2B both a cylindrical and a centric approach we proposed to create a digital transverse section using our 3D model. Our original 3D model generated in SPIERS had three things we needed to alter before we could do this. First, the model didn't consist of a single mesh but had numerous disarticulated parts. Second, the model was a skeletal outline of the specimen and was therefore hollow and non-manifold. Finally, fine details such as the outline of leaves and attachment to the base were fragmented and appeared pixelated due to the faint signal of organic material on the original peels. All of these limited our ability to produce an accurate digital transverse section. To overcome these limitations we used Blender to voxel remesh our original skeletal model, generating solid manifold meshes. The pixilated regions of the meshes were smoothed using a sculpting workflow, and any holes were filled in. Copies of the original SPIERS model were used to ensure the new meshes maintained the same convex hull profiles of the originals. (Fig. 3B). Using a Boolean operation we were then able to produce a digital transverse section at the shoot apex preserving leaf organization. We also used this opportunity to propose a realistic surface texture for what the plant would have looked like in life. Using a Canon EOS 5D Mark IV and a Canon EF 100mm f/2.8L Macro IS USM Lens,

and a Nikon SMZ18 with Schott VisiLED ring light we took images of the extant lycopod species *Lycopodium clavatum*. Using these images and hand sculpting of cell structure based on our previous investigation of *A. mackiei* (*15*) we proposed a surface texture of what *A. mackiei* would have looked like in life. A 3D interactive model of the specimen can be viewed on Sketchfab: https://sketchfab.com/3d-models/asteroxylon-mackiei-f090e445a53a47cd8b394b1ee7d9f517 (Password: Asteroxylon).

Quantification of phyllotaxis

We quantified phyllotaxis by characterizing contact parastichies (*1*, *4*). Contact parastichies are clockwise and anticlockwise spirals that connect neighboring leaves and are typically visualized on lattice diagrams (*1*). Lattice diagrams represent the positions of leaves as points and parastichies as lines or spirals. Phyllotaxis can be investigated with two approaches, the cylindrical approach and the centric approach. The cylindrical approach is used to visualize helices of leaves on the outer cylindrical surface of more mature areas of the shoot. The convention is to "unwrap" the cylinder allowing leaf arrangement to be represented on a 2D planar lattice. The helical parastichies connecting leaves can then be viewed as straight lines on the 2D lattice. In contrast, the centric approach is used to depict parastichies that radiate out from the shoot apex. On a centric lattice, parastichies connecting neighboring leaves can be viewed as spirals radiating out from the center of the meristem. Both a cylindrical and a centric approach were used to investigate phyllotaxis in *A. mackiei*. Taking a cylindrical approach with our *A. mackiei* 3D models in Blender, we first added bounding cylinders approximately the same diameter as our leafy shoots to each reconstruction. The positions of leaf bases were then marked onto these cylinders using the 'Draw' brush tool in Texture Paint mode. We next used the Blender 'Unwrap' option in the 'UV Mapping' menu to digitally 'unwrap' the cylinders to display leaf arrangement on a 2D plane. Lattice diagrams with contact parastichies manually annotated were then created based on the 'unwrapped' stem in Inkscape. The centric investigation was based on transverse sections of *A. mackiei* made close to shoot apices. For each transverse section the center of each leaf was represented by a point in the lattice. Contact parastichies connecting neighboring leaves were drawn on manually in Inkscape. The number of clockwise and anti-clockwise parastichies were counted to quantify phyllotaxis. When taking both the centric approach and the cylindrical approach we endeavored to use as many leaves as possible in our analysis and leaves excluded from our analysis are shown in figures (Fig. 1-4) for completeness. Leaves were excluded from the analysis for two main reasons. First, during the centric representation leaves at the center were excluded as these were smallest and most easily damaged or lost when making the thin sections. Omitting these leaves did not influence our investigation as the quantification of contact parastichies requires investigation of a number of well preserved leaves around the full circumference of the stem from which parastichies are traced towards the shoot apex, which we have present in all fossils examined. Text book examples of this approach, where the smallest developing organs at the shoot apex are omitted, include characterization of contact parastichies in sunflowers, rosette plants, cacti or pine cones (*4*, *31*), verifying our approach. Second, putative leaves that were damaged or lacked a clear attachment to the shoot were omitted from the cylindrical approach (Fig. 2, 4). All other leaves were included in our analyses.

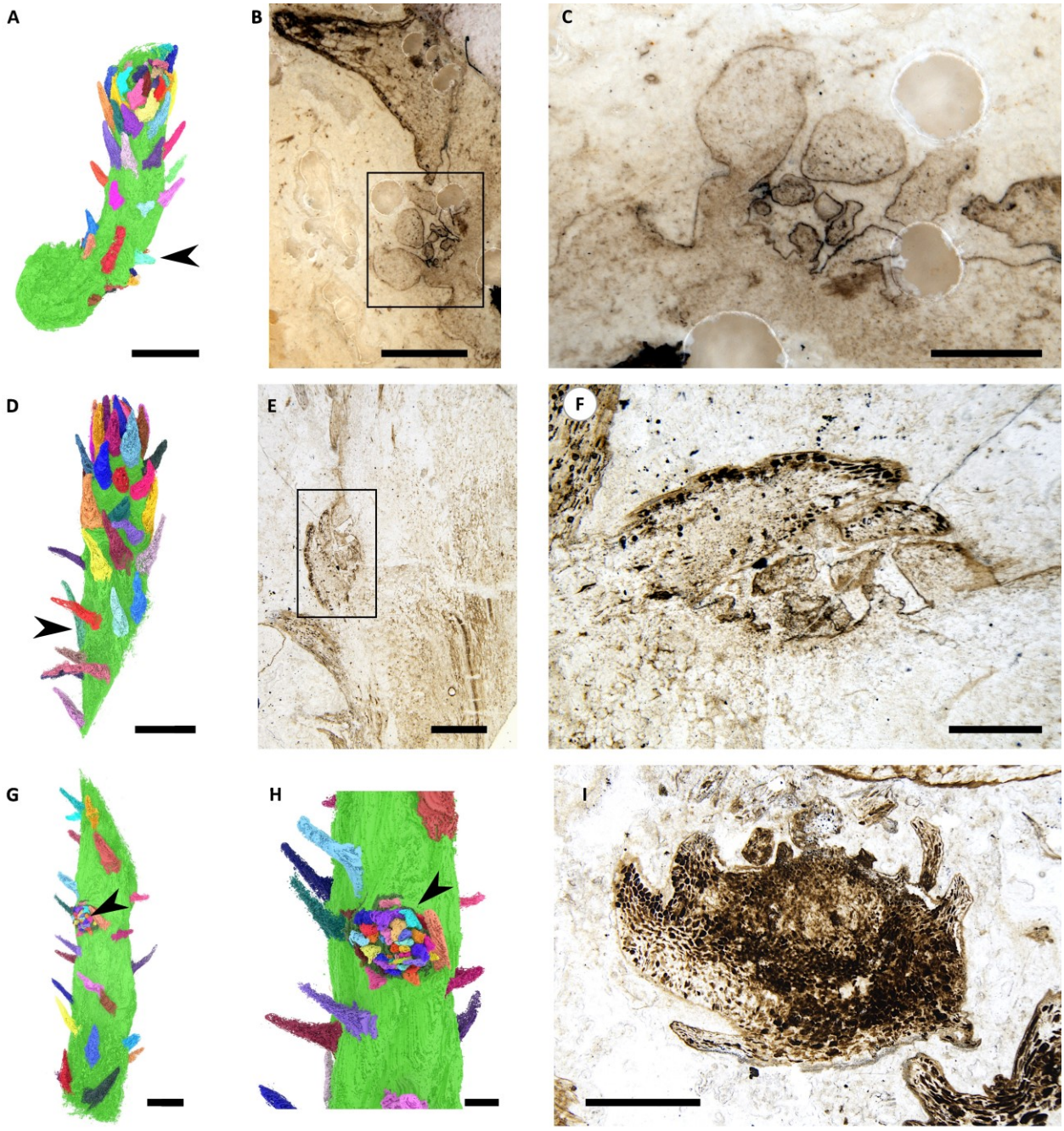


**Fig. S1. Presence of lateral buds on *A. mackiei* shoots.** (A, D, G, H) Position of buds marked with arrowheads. (B, C, E, F, I) Photographs of peels showing the bud regions. (B, E) Low magnification images showing the size of buds relative to leaves, inset boxes highlight the position of buds magnified in C and F. (I), photograph showing the bud region cut in transverse section when completely detached from the stem. Specimen accession code: A. Bhutta BL29A/75 (B, C), A. Bhutta 139A/28 (E, F), A. Bhutta BL29A/163 (I). Scale bars, 5 mm (A, D, G), 2 mm (H), 1mm, (B, E, I), 500 µm (C, F).

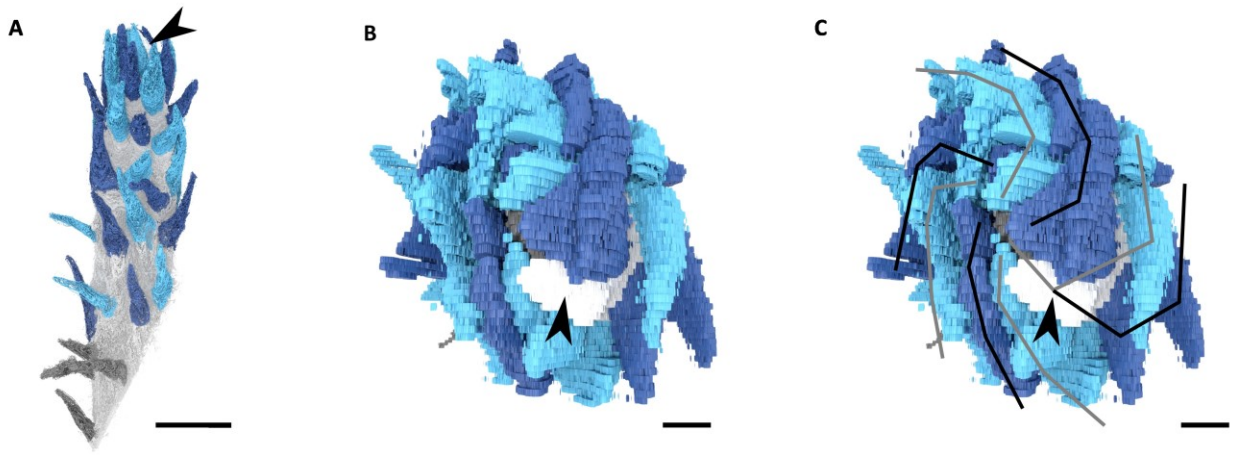


**Fig. S2. Anticlockwise contact parastichies showing branching of a parastichies at the apex. (A-C),** 3D reconstructions of *A. mackiei* leafy shoot apex (Fig. 2B) showing anticlockwise contact parastichies in light and dark blue, black arrowhead marks the position of the white leaf where the parastichies split in two. Position of the contact parastichies marked on with black and grey lines (C). Scale bars, 5 mm (A), 1 mm (B, C).

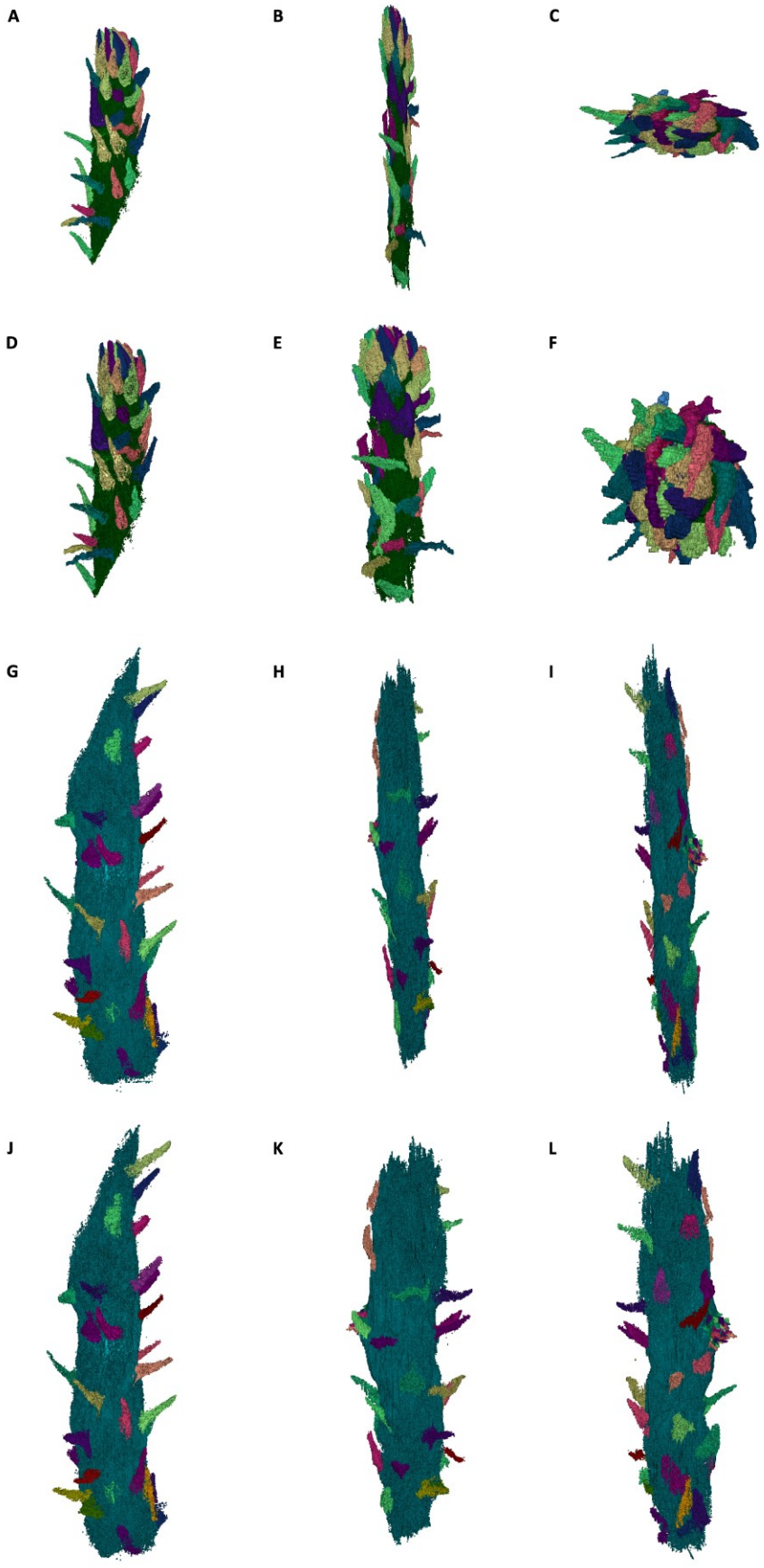
A
B
C
D
E
F
G
H
I
J
K
L

**Fig. S3. Stem thickness in 3D reconstructions. (A-L),** *A. mackiei* 3D reconstructions A-F (Fig. 2B) and G-L (Fig. 2C) viewed from three different angles using peel thicknesses based on either A. Bhutta's estimate (17) (A-C, G-I) or our calculated estimate (D-F, J-L). Reconstructions based on A. Bhutta's estimate (A-C, G-I), show significant flattening which is corrected for using our revised thickness estimates (D-F, J-L).

**Data S1. (Separate file)**
Excel spreadsheet describing the peels used to create each 3D reconstruction and our estimation of peel thicknesses.